Joint Communication and Bio-Sensing With Plasmonic Nano-Systems to Prevent the Spread of Infectious Diseases in the Internet of Nano-Bio Things

Amit Sangwan, *Member, IEEE*, and Josep Miquel Jornet, *Senior Member, IEEE*

***Abstract*— With the advances in nanotechnology, novel nanosensing technologies can play a pivotal role in today's society. Plasmonic sensing has demonstrated unprecedented detection reliability and resolution in a very compact form factor. Traditional plasmonic sensors leverage biofunctionalized metallic grating structures whose frequency response in transmission or reflection changes according to the presence of targeted biomarkers. However, these sensing setups require bulky measurement equipment to couple light to and from sensors for excitation and detection. In parallel, for over a decade, the nanoscale electromagnetic communication community has been leveraging plasmonic structures to transmit information at the nanoscale efficiently. By combining the two realms, this paper proposes the concept of joint nanoscale communication and bio-sensing systems enabled by plasmonic sensing nanoantennas. Sensing nanonodes can communicate from nanonode to nanonode for intra-body networks and from nanonode to a wearable device which, by leveraging the edge, can process and transmit the sensing information to the cloud, resulting in accurate diagnosis and reduced load on the medical testing infrastructure. First, we model the changes in the frequency response of a biofunctionalized plasmonic nanoantenna when exposed to different biomarkers. Then, we propose a chirp-spread spectrum excitation and detection system to enable simultaneous communication and sensing at the nanoscale. We present a data-driven human tissue model for communication through human tissue. We also present numerical results to demonstrate the performance of the proposed system.**

***Index Terms*— Nano communications, nano sensing antenna, nanonetworks, Internet of Nano-Things, biosensing.**

I. Introduction

With technological advances in science and technology, we are in most ever connected era of human society history. We live in a society where information travels at the speed of light, and traveling is easier than it ever has been in history. In such a dynamic paradigm, early pathogen detection and diagnosis are the key to defer the next pandemic in such a connected world. Traditionally, pathogen detection has been performed by using several sensing mechanisms [2], [3] such as color-changing chemical titration, microscopy, spectrometry, and recent RNA/DNA based detection schemes [4].

In parallel to these techniques, plasmonic sensing is an upcoming sensing technology that promises unprecedented accuracy for biomarker detection [5], [6], [7]. Plasmonic sensing leverages molecular interactions at the nanoscale and bridges that with the macro world using light as an information carrier. Light, i.e., electromagnetic radiation in the optical spectrum, is utilized because its small wavelength enables molecular scale interactions with matter. Plasmonic nanostructures are designed to couple the incident light into plasmonic waves on metallic-dielectric interfaces. These plasmonic surface waves are sensitive to the surface structure properties and are therefore leveraged for sensing. The surface is made biomarker selective using molecular engineering where a biofunctionalized molecular layer is deposited on this plasmonic surface. The biofunctionalized layer binds only to the biomarker of interest and offers very high selectivity. This unprecedented selectivity allows for accurate detection at an ultra-low concentration.

Despite the unique capabilities of plasmonic sensors for biomarker detection and selectivity, currently, bulky test equipment is needed to interrogate the sensors, limiting their practical application. In parallel to these advances in sensing technology, nanostructural engineering and nanophotonic designs are also advancing the optical technology to nanoscale applications. In the last decade, lasing devices with ultra small footprints [8], [9], on-chip waveguides [10], plasmonic waveguides [11], [12], [13], power-splitters [14], phase shifters [15], [16], nano-antennas [17], [18], [19], [20] and metamaterials [21], [22], [23] have enabled unprecedented nanophotonic advancements. While most of these technologies aim at solving communication bottlenecks by enabling ultra-compact broadband communication, these can be tailored to support nanoscale sensing applications.

Besides light-based nano-sensing, nanoscale communication has become an emerging field that can be leveraged to communicate intrabody nanomachine to nanomachine or implanted nanomachine to wearable [24]. For such communications,

Manuscript received 30 January 2022; revised 11 May 2022; accepted 16 June 2022. Date of publication 14 October 2022; date of current version 14 November 2022. This work was supported by the U.S. National Science Foundation (NSF) under Grant IIP-1718177, Grant CBET-1706050, and Grant CBET-2039189. An earlier version of this paper was presented at the Proceedings of the Eight Annual ACM International Conference on Nanoscale Computing and Communication [DOI: 10.1145/3477206.3477447]. *(Corresponding author: Amit Sangwan.)*

The authors are with Department of Electrical and Computer Engineering, Northeastern University, Boston, MA 02115 USA (e-mail: amit@northeastern.edu).

Color versions of one or more figures in this article are available at https://doi.org/10.1109/JSAC.2022.3214288.

Digital Object Identifier 10.1109/JSAC.2022.3214288

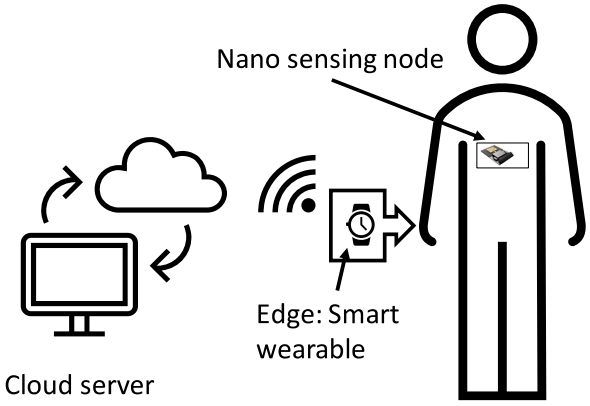

Fig. 1. Edge computing with internet of nano-bio things.

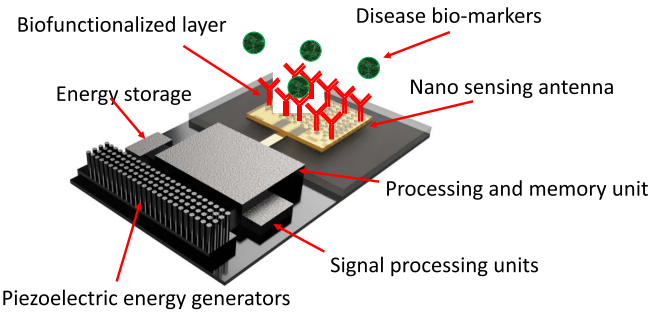

Fig. 2. Concept of plasmonic nano-patch antenna as a biofunctionalized sensor.

different technologies are proposed such as galvanic coupling [25], [26], ultrasound waves [27], [28], electromagnetic waves in radio frequency band [29], terahertz band [30] and optical band [31], [32] as well as molecular communications [33], [34]. Together, the aim has been to enable an Internet of Nano-Bio Things [35] that bridges the macro world in which we live with the biological world inside our body. This opens the door to unprecedentedly precise sensing of disease biomarkers and real-time recovery monitoring and, ultimately, the next wave in healthcare technology that bridges the nano-bio scale with the power of cloud computing through edge networks. Such systems promise timely diagnosis, real-time monitoring and will play a key role in early-detection of infectious diseases and mitigating future pandemics. Nevertheless, while these technologies provide a roadmap for the future of Internet of Nano-Bio Things, the technological bridges that can translate these models into real nano-device designs have been missing.

In this paper, we present a plasmonic nanoantenna that can also work as a biofunctionalized sensor to bridge the gap of the nanosensing device and nanoscale intra-body communications. The proposed plasmonic nanosensing system shown in Fig. 2 allows for simultaneous wireless bio-sensing and nano-communication in a compact footprint. For sensing the proposed antenna is coated with a biofunctionalized layer that binds to a disease-specific biomarker and changes the antenna response. To work in conjunction with nanoantenna, we propose the adoption of chirp spread spectrum (CSS) to simultaneously extract the sensing response and perform communication between intrabody nanonodes and wearables. The wearable can perform computation at the edge to extract the sensing features and transmit the relevant data to the cloud as shown in Fig. 1. Along with system design, we also present a detailed analysis of the sensing performance of the biofunctionalized nanoantenna and the bit error rate analysis of the communication link from nanonode to wearable using the CSS.

The remainder of the paper is organized as follows. In Sec. II, we present the relevant related work focusing on the human tissue channel model for optical signals, plasmonic biosensors, biofunctionalization and joint communication and sensing. In Sec. III, we present the design of an optical nanoantenna. In Sec. IV, we evaluate the performance of the nano-patch antenna as a biosensor. In Sec. V, we present the design of the chirp waveform signal to extract the sensing information and carry the data. In Sec. VI, we present the channel model for sensor – sensor and sensor – wearable device. In Sec. VII, we present the detection mechanism that can leverage the chirp waveform and the antenna response for performing sensing detection along with joint communication packet decoding. In Sec. VIII, we perform the communication link analysis for different scenarios and model factors such as channel and noise on the received signal and bit error rate. In Sec. IX, we present the numerical analysis results showcasing the results from the analytical and numerical models, and in Sec. X, we conclude the study by highlighting key results and the future work.

II. Relevant Works

A. Human Tissue Model

Many research groups have modeled human tissue as the channel for optical signal propagation [36], [37], [38]. These works rely on experimental data and the spectrometric analysis of tissue types such as skin, blood, adipose, muscle, brain tissue, and melanin concentrations. While many of these measured properties help model human tissues to some degree, in reality these models have large variance and any multi-layer or bulk tissue model without some modification can not perfectly fit all humans. This is because the composition of human body varies from person to person. However, we can make a fair approximation to guide the engineering design with factors such as layer thickness and concentration [39], [40], [41]. The concentrations of factors such as fat [42], melanin content [39], [40], and blood concentration [38], [43], [44] affect the optical signal propagation. For the special case of optical communication at nanoscale, along with these factors, non-homogeneity of the tissues and cellular composition also affects the signal propagation making it even more challenging to predict the response. Some works have attempted to create models that aim to target such nanoscale communication links [45], [46] for cell-cell or nanomachine-cell interactions.

B. Plasmonic Biosensors

Plasmonic biosensors have been an active area of research in last decade and there has been a myriad of advances

made in this field. Plasmonic biosensing relies on plasmon polariton waves which can be excited using a prism and coupling the light in reflection from the sensor. The surface of a plasmonic sensor is coated with biofunctionalized layer that binds to target molecule and changes structure resonance. This effect is then detected in reflection or transmittance to perform sensing. Plasmonic biosensing can be performed using different mechanisms: Surface plasmon resonance(SPR) sensing, localized surface plasmon resonance (LSPR) biosensing, Chiral plasmonic biosensing, Magnetoplasmonic biosensing, and Quantum plasmonic biosensing [5], [47], [48], [49], [50].

The LSPR biosensing is done using subwavelength particles [51], which due to the small size, are more sensitive to their surrounding media properties [52]. Traditionally they have been used to enhance the spectroscopic measurements such as in surface-enhanced infrared absorption spectroscopy [53], surface-enhanced Raman scattering, surface-enhanced fluorescence [54], [55], and by detecting a shift in absorption spectra(sensitive to surrounding molecules) [52], [56].

Chiral plasmonic bio-sensing relies on the fact that chiral symmetry causes different absorption for right-hand circularly polarized light and left-hand circularly polarized light. This difference can be leveraged at the plasmonic level to identify the mechanisms of chiral bioactivity in proteins [57], [58], [59], [60]. Chiral plasmonic has therefore become an active area of research to develop chiral sensitive plasmonic structures for sensing in visible and NIR region.

Magnetoplasmonics biosensing relies on magnetic nanoparticles and magneto-optical structures to amplify surface plasmon polariton waves. These merged effects of plasmonic with magneto-optics are called magnetoplasmonics. They have gained their popularity for in-vitro sensing and bio-imaging applications [61], [62], [63].

Quantum plasmonic biosensing tries to overcome the fundamental limit of plasmonic waves carrying information. By using the quantum properties of light, such as quantum correlation, and shielding, the information carried from the noise floor is defined by the shot-noise limit defined by the Heisenberg uncertainty principle [64], [65]. In addition to these types, there have been demonstrations of sensing based on functionalized graphene nanoribbon based biosensors [66], biofunctionalized optical waveguide-based plasmonics sensors [67] and biofunctionalized field effect transistor channel biosensors [68] that leverage plasmonics to perform sensing.

C. Biofunctionalization

Plasmonic biosensors are sensitive to their surrounding layers, and to make them sensitive to a particular biomarker, they need to be coated with a biofunctionalized layer. The binding process results in a change of physical properties such as refractive index, conductivity, or pH value, among others. These changes influence the resonance frequency of the SPR sensor. The successful coating of an SPR sensor with a biofunctionalized layer requires two main components, namely, a primer layer and a biofunctionalized layer. The primer binds to the metal surface of the sensor and allows the biomarker selective coating to bind reliably on the sensor.

Based on their type of binding, sensors can be classified into four categories: DNA-, immuno-, cell-, antigen- and imprinting-based sensors [47], [69]. DNA-based sensing leverages single-stranded DNA (ssDNA) and its affinity to bind with the virus. A layer of ssDNA with preserved reactivity towards the host-virus is deposited on the SPR. Such ssDNA layer is carefully designed to be stable and relies on nucleic acid hybridization. Peptide nucleic acids, which are structurally similar to DNA, have also proved to be a promising candidate for DNA detection [70], [71].

Immunosensors rely on using the antigens created by the bodies in response to the virus for detection. These antigens have a higher affinity for the virus proteins and thus bind with them, similar to a lock-key mechanism. Such binding results in the change of the structural properties of the surface layer, which changes the response of the SPR sensor, thus allowing for the detection by an optical signal transmitted or reflected by the sensor. To reduce dependency on the immune-generated antigens, active research is going on to develop DNA and peptide aptamers that resemble immune-generated antigens, which have been demonstrated for the detection of viruses [72], [73]. Antigen-based sensors work on the principle of coating the surface with a virus, and when the antigens come in contact with the surface, they change the surface properties. For testing such sensors, antigens are extracted from an infected person's serum. These sensors are limited by the concentration of antigens produced by the person at different stages of infection. These types of sensors are currently limited to out-of-body testing in laboratory setups.

Cell-based sensors cover the surface of the sensor with the host cells. When the virus attaches and infects the cell, it causes the changes, thus providing the ability to analyze cytopathic effects [74]. These sensors provide an alternative to studying viral infections other than hosts or animals.

Imprinting-based sensors rely on using the molecular imprinted polymers, which are synthetically designed to provide complimentary vacancies in the polymer matrix that allows for the deposition of the target antibody or virus on the surface. These perform similar to the biological methods of detection but improve on increasing reliability and function in harsh operating environments with re-usability and reduced cost [75], [76].

It is essential to note that biosensors can be impacted by other elements besides their target biomarker. More specifically, while they might not chemically react, other blood components, including red and white blood cells and platelets, might obstruct the implant. Correspondingly, sensor defouling and reusability are currently at the center of several studies, and multiple different methods have been proposed, from ultrasonic cleaning to electrochemical defouling [77], [78], [79].

D. Joint Communication and Sensing

Joint communication and sensing have recently gained popularity in the context of 5G and even 6G networks. Mainly, in joint communications and sensing systems, the

same hardware, the same spectrum, and ultimately, the same signals are utilized to both carry information from the transmitter to the receiver while performing radar, i.e., extracting information from the channel itself [80], [81]. These types of systems leverage properties of signal propagation for multipurpose applications [82], [83], [84], [85]. However, other sensing methods utilize the communication channel changes for sensing, such as optical fiber-based earthquake detection [86], [87], [88] and waveguide-based optical sensing [67], [89], [90], [91]. With some known properties about the channel, they all rely on the spectrographic properties of the molecules composing the channel and try to predict the presence of a certain molecule based on its band of absorption. These systems rely on a relatively wide band transmitter and a sensitive detector that can sweep across the band of interest accurately for valid detection signals. Traditionally, these sensing measurements were performed by spectrometers, but with advances in device technology and the access to low-cost high-quality sources and detectors widely available for communications, we can perform these measurements using the communication equipment.

III. Nano Antenna Design

Optical nanoantennas are functionally similar to their radio-frequency counterparts. They rely on the electromagnetic (EM) wave propagation length and the resonating structural parameters. However, materials such as metals, which are perfect electric conductors at radio frequencies, do not behave as perfect electric conductors at optical frequencies. These material properties influence the EM wave propagation inside the material and thus the overall geometry of the resonating structure.

A. Plasmonic Properties of Metals at Optical Frequencies

At optical frequencies, metals exhibit complex frequency-dependent conductivity. This complex conductivity arises/originates from the plasmon polariton waves on metal-dielectric interfaces. Plasmon waves are surface waves that exist in the electron cloud of the metal present on the metal-dielectric interface. These oscillations and their effect on the permittivity of the metal can be represented by the Drude-Lorentz model as [92]:

$$\varepsilon_m = \left[\varepsilon_m(\infty) - \frac{\omega_p^2 \tau_d^2}{1+\omega^2\tau_d^2} + j\frac{\omega_p^2 \tau_d}{\omega\left(1+\omega^2\tau_d^2\right)}\right], \tag{1}$$

where ε_m is the permittivity of the metal, ω_p is the plasma frequency of the material, τ_d is the electron relaxation time, $\epsilon_m(\infty)$ is the high frequency dielectric constant and $\omega = 2\pi f$ is the angular frequency.

Using this complex conductivity model, the propagation wave vector k_{spp} can be calculated accounting for the dispersion along the structure as per equation [92]:

$$k_{spp} = \left(\varepsilon_1\varepsilon_3 S_3^2 + \varepsilon_m^2 S_2 S_3\right)\tanh\left(S_2 h\right) + \varepsilon_m S_2\left(\varepsilon_3 S_1 + \varepsilon_1 S_3\right) \tag{2}$$

$$S_1 = \sqrt{\beta^2 - \varepsilon_1 k_0^2}, \tag{3}$$

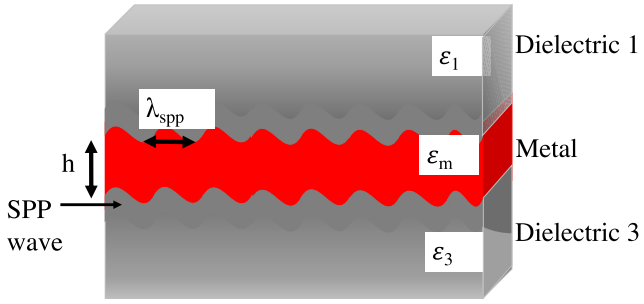

Fig. 3. SPP waves at metal-dielectric-metal interfaces for thin metal.

$$S_2 = \sqrt{\beta^2 - \varepsilon_m k_0^2}, \tag{4}$$

$$S_3 = \sqrt{\beta^2 - \varepsilon_3 k_0^2}, \tag{5}$$

where $k_0 = \omega/c$ is the free space vector, β stands for the complex propagation constant parallel to the surface, ε_1 and ε_3 are the permittivity of the layers surrounding the metal sheet, and ε_m is the permittivity of the metal as described in (1). Using k_{spp}, we can calculate the plasmonic wavelength using the relation:

$$\lambda_{spp} = \frac{2\pi}{\Re\left\{k_{spp}\right\}}. \tag{6}$$

At optical frequencies, λ_{spp} governs the antenna design equations instead of the free space wavelength.

Therefore, it is established that the resonating frequency of our antenna is sensitive to not only the structure length but also to the surrounding material properties. This property can be harnessed for sensing. Sec. IV presents further details on the performance of such a plasmonic antenna as a sensor.

B. Optical Nano-Patch Design

Patch antennas have become a popular choice for design in modern wireless applications. One of the main advantages a patch antenna offers is its flat design which makes it suitable to be produced on a mass scale with reliable manufacturing processes such as integration with printed circuits. Even at the nanoscale, flat designs allow for easier fabrication by using techniques such as metal deposition, masking, and etching.

A patch antenna design consists of three main components, a meticulously designed resonating patch, a ground plane, and a dielectric material in between the patch and ground plane. The geometry of patch is a deciding factor for its resonating frequency, and for perfect conductors is usually in the range of $L > \lambda_0/3$ and $L < \lambda_0/2$ [93], where λ_0 is the free-space design wavelength. However, the E-field distribution between ground plane and the patch is affected by the dielectric material properties. Therefore, a patch antenna resonance is highly sensitive to the surrounding dielectric properties. Patch antennas are usually designed to function as broadside radiators, radiating maximum power perpendicular to the antenna plane. However, with a careful selection of excitation mode and design parameters, they can also be designed as end-fire radiators, radiating maximum power in the direction of the antenna plane.

TABLE I

DESIGN PARAMETERS OF AN OPTICAL GOLD NANO-PATCH ANTENNA RESONANT AT 200 THZ

Parameter	Value
Patch Length	370 nm
Patch Width	300 nm
Stub Length	60 nm
Stub Width	10 nm
Substrate Thickness	50 nm
Antenna Thickness	20 nm
Plasma Frequency	13.35 PHz

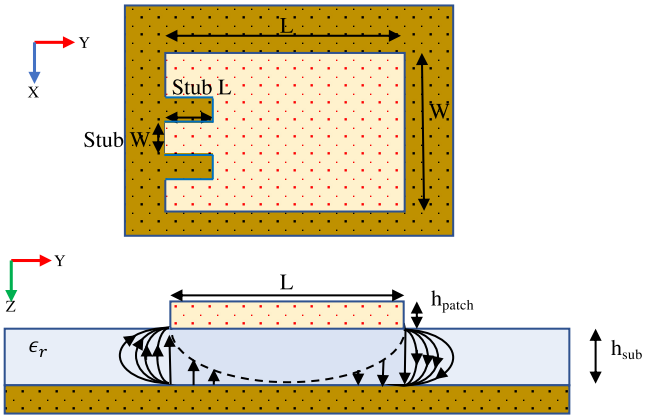

Fig. 4. Geometry of a patch antenna.

Unlike dipole antennas, there is no closed-form expression to dictate the patch antenna geometry. However, there are models that approximate these dimensions, such as cavity model [93] but these models rely on assumptions that antenna material is a perfect electric conductor and fail to account for phenomena such as plasmonic waves on the antenna-dielectric surface and Fabry-Perot effect from the patch-ground plane cavity. Due to the complexity of formulating these models analytically, FEM analysis is often used as a standard practice to design and predict patch antenna performance.

In this study, we utilize finite-element methods (FEM) with COMSOL Multiphysics to design and model patch antennas at optical frequencies. We model the active antenna element and the ground plane with the complex-valued material properties of gold. The dielectric substrate sandwiched between the ground plane, and the patch is chosen to be of dielectric constant $\epsilon_r = 4$ ($\sim$ Dielectric constant of $SiO_2 = 3.9$). We utilize the antenna performance parameter S11 as the objective function and perform parametric sweeps across antenna length, width, and thickness to minimize the reflection losses of design frequency and maximize radiated signal. We select an operating frequency of 200 THz, which corresponds to the popular telecommunication wavelength of 1500 nm, commonly adopted in fiber-optical systems and for which many of the aforementioned technologies have been developed. The final design parameters are presented in Table I and the resulting S11 parameters are shown in Fig. 5.

IV. NANO-PATCH ANTENNA AS A BIOSENSOR

A biosensor is basically a transducer that converts one form of bio-signal into another form which can be extracted and analyzed to perform detection. Most existing sensors convert the measured bio-signal into a change in properties such as electric/optical conductance, reflected signal, or chemical binding properties. Localized surface plasmonic sensors transduce the detection results into a difference in their resonating frequency, which can be read in reflection, transmittance, or conductance [5], [6], [7]. To perform detection, these sensors are coated with a bio-functionalized layer that binds to the biomarkers of interest. This binding results in a change in their surface properties which affects the propagation of plasmonic waves on the sensor surface.

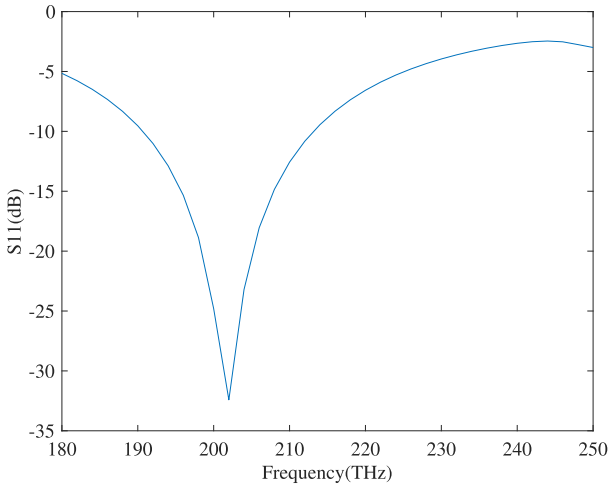

Fig. 5. S11 parameter of the reference nano-patch antenna.

Generally, an antenna is designed to resonate at the desired frequency. However, in the case of a plasmonic antenna, this frequency can significantly change based on the properties of its surrounding material. This phenomenon offers an unprecedented way to accurately sense the environment with an existing antenna geometry. By biofunctionalized the antenna itself, when the target biomarker is present, both the electrical properties of the antenna building material and the thickness itself change. By tracking those changes, detection is performed.

Modeling a particular biomarker and the corresponding biofunctionalized layer would require an extensive study of the material properties, which is part of many ongoing works [47], [69]. Meanwhile, to analyze the detection performance of our designed patch antenna, we model these effects in FEM analysis with a parameter sweep. Figure 6a presents the impact of change in the antenna patch thickness on the resonant frequency of the antenna. Patch thickness is varied in steps of 5 nm, and the results demonstrate that the antenna's resonating frequency is highly susceptible to these minor changes in thickness. While Fig. 6b shows the effect of change in the dielectric properties ($\epsilon = 1 - 2.25$) of the material on top of the patch affecting the resonating frequency of the antenna. These results demonstrate the ability of the designed optical nano patch antenna to function as a biosensor.

V. ANTENNA EXCITATION SIGNAL WAVEFORM DESIGN

To extract the sensing information from the antenna, a wideband waveform that spans all the possible resonant frequencies of the antenna when sensing should be used. Considering the

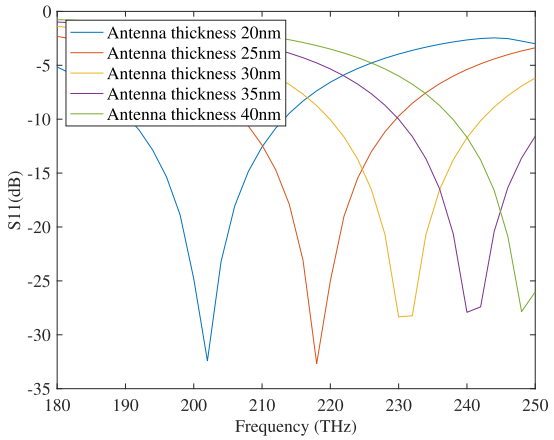

(a) S11 parameter as a function of frequency for different antenna top layer thickness h_{patch}.

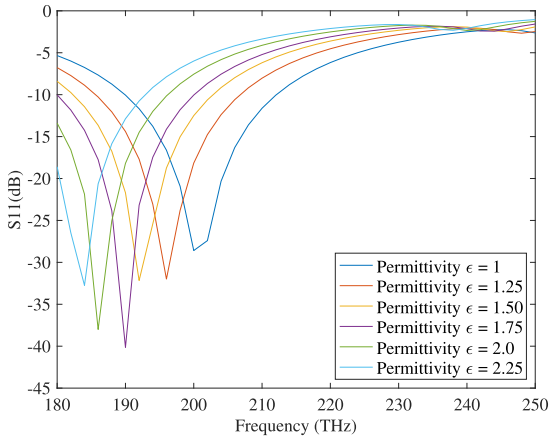

(b) S11 parameter as a function of frequency for different top dielectric layer permittivity.

Fig. 6. Sensing performance analysis of optical patch antenna.

limited capabilities of a nanomachine, we propose using a frequency-sweeping chirp signal. The simplest chirp waveform is the linear chirp signal, in which the frequency increases with time (up chirp) or decreases with time (down chirp). Chirp waveforms have been widely used for sensing, as the multi frequencies translate to multi-resolution sensing [94], [95], [96]. Chirp waveforms offer several advantages for communications, such as immunity to channel frequency selectivity [97].

A chirp signal in time domain is defined as

$$x(t) = \sin\left(\phi_0 + 2\pi f(t)t\right), \tag{7}$$

where ϕ_0 is the initial phase of the signal and

$$f(t) = Ct/2 + f_{start}, \tag{8}$$

where C is the chirp rate/slope and f_{start} is the starting frequency. For linear chirp signals,

$$C = \left(f_{stop} - f_{start}\right)/T, \tag{9}$$

where f_{stop} is the chirp stop frequency and f_{start} is the chirp start frequency and T is the time of sweep.

When this sweeping chirp signal is transmitted through the antenna, the antenna response is imprinted on it, which can be used for sensing. The power spectral density P_t of the imprinted transmitted signal is given by

$$P_t\left(f\right) = P_{chirp}\left(f\right)\left(1 - \left|R_{ant}\left(f\right)\right|^2\right), \tag{10}$$

where P_{chirp} is the power spectral density of generated chirp signal and R_{ant} is the antenna input reflection coefficient or S11 parameter and depends on the sensed information, as described in Sec. IV.

TABLE II
REFRACTIVE INDEX OF TISSUE IN OPTICAL BAND 400 NM - 2000 NM

Layer	Value(n)
Air	1
Skin tissue [37], [98]	1.41
Adipose tissue [37], [99]	1.44
Blood (98% oxygenated) [44]	1.37

VI. CHANNEL MODEL

To effectively model the communication performance for the proposed joint sensing and communication system, an accurate channel model is needed. In our analysis, we consider two scenarios: A) Nano-sensor to nano-sensor link and B) Nano-sensor to wearable link. The channel losses can be classified as the combination of the following phenomena:

- **Reflective loss:** This is the result of the refractive index mismatch between the different tissue layers in the body. These losses can be modeled using the following equation:

$$L_{Ref}(\lambda) = \left(\frac{\left|n_1\left(\lambda\right) - n_2\left(\lambda\right)\right|}{n_1\left(\lambda\right) + n_2\left(\lambda\right)}\right)^2, \tag{11}$$

  where n_1 and n_2 stand for the refractive index of Layer 1 and Layer 2, respectively. The refractive index of different tissue types for the wavelengths λ of interest is summarized in Table II.
- **Scattering and absorption loss:** These losses account for the absorption and scattering from the medium. A general calculation for scattering and absorption losses can be performed using the equation:

$$L_{ScaAbs}(\lambda, d) = \exp((\mu_{scr}\left(\lambda\right) + \mu_{abs}\left(\lambda\right))d), \tag{12}$$

  where μ_{scr} is the scattering coefficient, μ_{abs} is absorption coefficient and d is the distance/layer thickness. The absorption and scattering properties (μ_{scr} and μ_{abs}) are compiled from literature. For the 400 nm - 2000 nm band, plots of absorption and spreading coefficients for blood (for 98% oxygenated blood) [38], adipose tissue [37], [100] and skin (for low-melanin skin) [37], [100] are shown in Figs. 7a, 7b, and 7c, respectively.
- **Spreading loss:** This captures the fact that the signal propagates as a wave and spreads into the medium. This can be calculated using the equation:

$$L_{Spr}\left(\lambda, d\right) = \left(D\left(\frac{\lambda^2}{4\pi}\right)\left(\frac{1}{4\pi d^2}\right)\right)^{-1}, \tag{13}$$

  where d is the distance from the radiation source, D is the directivity gain ($D = 4\pi/\Omega_A$), for a point directional

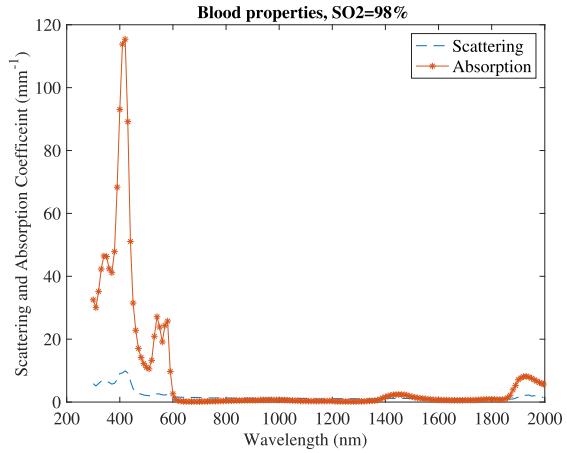

(a) Scattering and absorption coefficient of whole blood in optical band 400 nm - 2000 nm.

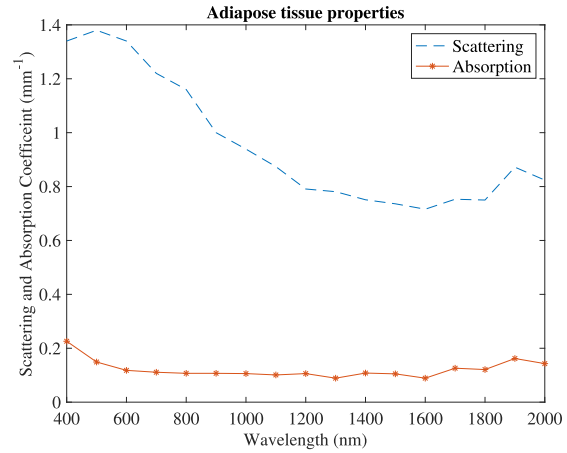

(b) Scattering and absorption coefficient of adipose tissue in optical band 400 nm - 2000 nm.

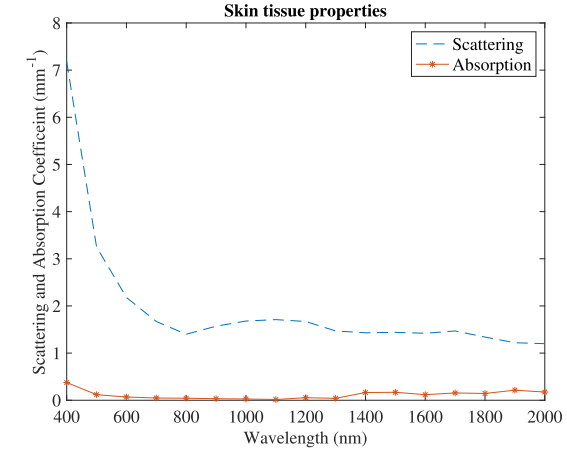

(c) Scattering and absorption coefficient of skin tissue in optical band 400 nm - 2000 nm.

Fig. 7. Scattering and absorption properties of different human tissue layered channel.

source such as a laser emitting with the radiated beam angle θ and ϕ, the directivity D can be expressed as:

$$D = \int_{\theta=0}^{\Delta\theta} \int_{\phi=0}^{\Delta\phi} \sin\theta d\phi d\theta = \Delta\phi(1 - \cos\Delta\theta). \quad (14)$$

- **Total loss:** All the previous losses in dB can be added to obtain the total loss suffered by the signal as:

$$L_{total}(\lambda, d)\,[dB] = 10\log\left(L_{Ref}(\lambda, d)\right.$$

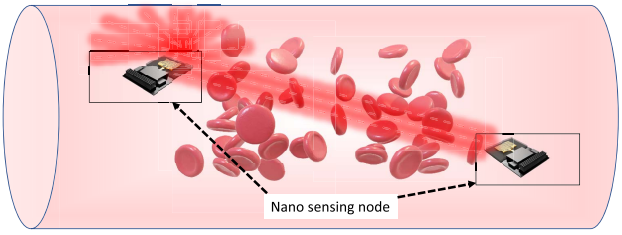

(a) Sensor to sensor communication through blood. Scenario representing 2 sensors flowing through a blood vessel.

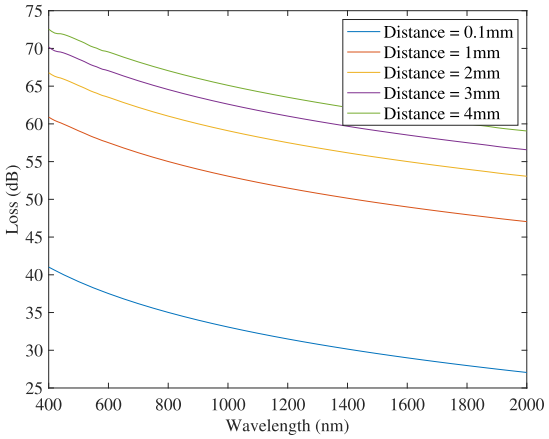

(b) Total channel loss computed for sensor to sensor link in blood for different inter-node distances.

Fig. 8. Sensor–sensor communication scenario with blood as channel.

$$\times\ L_{ScaAbs}(\lambda, d)\, L_{Spr}(\lambda, d)). \quad (15)$$

This total channel loss is a frequency dependent and can be used to calculate the channel transfer function $(H(f))$.

A. Sensor to Sensor

For the sensor to sensor channel model, we can assume the sensors to be in different tissues, and thus we can create multiple cases. For this analysis, we performed analytical calculations for 2 cases: Blood and Adipose(Fat) tissue.

Case 1 is to imagine the sensors are flowing in the bloodstream, as shown in Fig. 8a. In this case, we can model the channel as per the optical properties of blood as shown in Fig. 7a to compute scattering and absorption loss. Then total loss can be computed using (15), which is shown in Fig. 8b. For modeling the channel response, we accounted for the part where we used the distance as the main factor, for such high frequencies and the bandwidth, the effect of relative flow and speed difference will be minimal. Hence, the attenuation of the signal by the channel itself is the major factor affecting the signal, and the model follows that. However, to expand the model into a more practical application, an application-specific model needs to be developed, which accounts for the right variables of mobility and CSI to predict performance.

Case 2 is when nanosensors are implanted in the fat layer of the human tissue and there is an adipose fat layer between them as shown in Fig. 9a. Using the adipose tissue properties from Fig. 7b and Table II, we can calculate the total loss

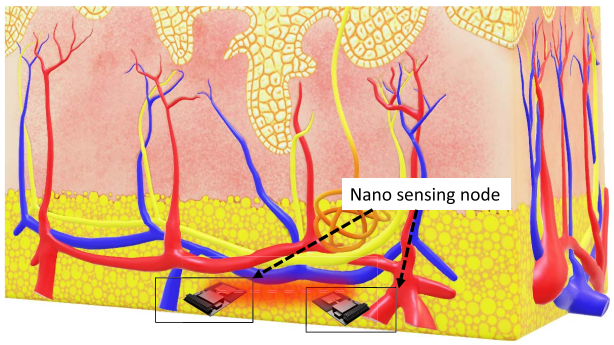

(a) Sensor to sensor communication through adipose tissue. Scenario representing 2 sensors communicating through adipose tissue.

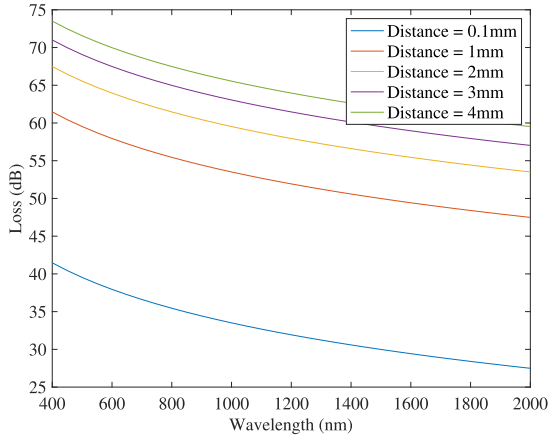

(b) Total channel loss computed for sensor to sensor link in adipose tissue for different inter-node distances.

Fig. 9. Sensor–sensor communication scenario with adipose tissue as channel.

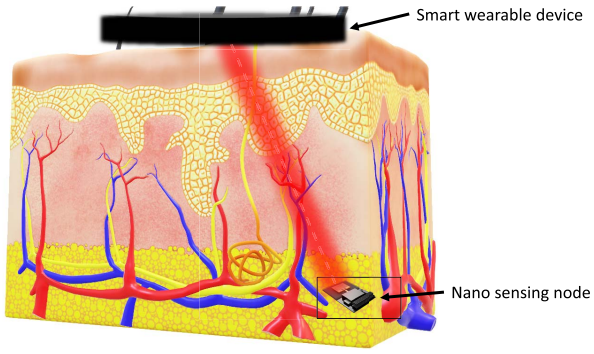

(a) Illustration representing sensor to wearable communication through different layers of skin tissues.

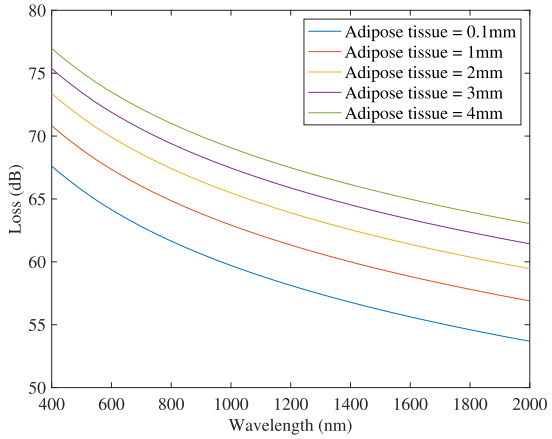

(b) Total channel loss computed for wearable to sensor link through multiplayer tissue model with different thickness of adipose tissues.

Fig. 10. Sensor–wearable communication scenario with multi-layer tissue model.

using (15). This loss is plotted in Fig. 9b for different distances.

B. Sensor to Wearable

For the sensor to wearable communication, we have to consider the bulk tissue layered model as discussed in several earlier works [35], [45], [101]. For this analysis, we can consider the bulk tissue to be a collection of different layers and calculate the collective losses from each layer.

For the multi-layer model, the different thickness of the tissue layer used are as follows: Air gap = 1 mm, Skin tissue = 1 mm, Adipose tissue = (0.1 mm -5 mm), Blood = 0.25 mm.

Losses from different tissue as per the model shown in Fig. 10a are calculated and presented in Fig. 10b with a common case of different adipose tissue thicknesses. On comparing results from Figure 8, 9 and 10, it can be observed that the losses for a particular distance are close. First the scale is on log to highlight clearly the change. For reference, 3 dB is half the power. And Second, overall we observe that spreading loss accounts for majority of the computed loss for the distance. For the given distance range of mm, comparing that to wavelength of few nm, it is very large. Assuming uni-directional antenna and no gains these losses account for majority of loss. For example, we calculate $\sim 64dB$ of spreading loss from 0.1 mm of distance, assuming no gains and unidirectional radiators.

VII. Detection Mechanisms

The generated wideband chirp signal is transmitted through the antenna. During transmission, the antenna frequency response is imprinted onto the signal, which now carries the information of the antenna resonant frequency. Simply stated, the maximum power of the transmitted signal is at the antenna resonant frequency. As discussed in Sec. IV, for an antenna working as a biosensor, the shift in resonant frequency plays a significant role. Thus, a mechanism to detect the peak power of the received signal is needed to extract the sensing information. Detection of peak power can be performed using different approaches. A wideband power spectrum of the received signal can be plotted and used to detect peak power. However, the computational complexity of such a mechanism makes it a challenge to implement in a nanomachine.

Instead, we propose the use of multiple antenna elements and a power comparator setup as shown in Fig. 11, similar to those proposed in cooperative spectroscopy [102]. In this detection method, the received signal is passed through two narrow-band antennas. One resonant at non-binding frequency (f_0) of the patch and another antenna resonant at binding frequency (f_1) of the patch. The received signal from both narrowband antennas is then fed to the power comparator, and if the power at f_0 is greater than the power at f_1, we can deduce that biomarker is absent. While if the power received

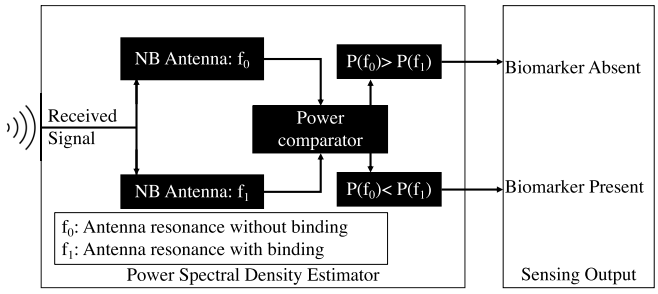

Fig. 11. Block diagram of power spectral density estimator of the proposed system for detection and calculating sensing output in a nanomachine.

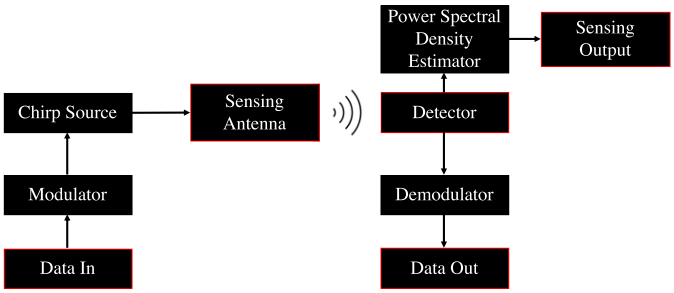

Fig. 12. Block diagram of the proposed system for detection and communication.

at f_1 is greater than the power at f_0, we can conclude that biomarker is present.

This sensing mechanism can be implemented parallel to the communication system, as shown in Fig. 12. Thus, communications and sensing can be simultaneously performed in the system.

VIII. Communication Link Model

With all the building blocks already defined, the communication link is modeled as follows.

A. Transmitter

A chirp signal is generated as per (7) and radiated by the antenna. Antenna reflection coefficient can be used to derive the antenna transfer function $H_{ant}(f)$ and transmitted signal can be as$X_{transmit}(f) = X(f)H_{ant}(f)$, where $X(f)$ is the frequency domain representation of $x(t)$. The power of transmitted signal can be calculated using (10).

B. Channel

The primary channel for the communication link is computed from the human tissue layers model. The total losses are computed using (15). For the bit error rate (BER) analysis, we focus on the wearable to sensor channel shown in Fig. 10b. By considering the frequency selective response of the channel, the power of the receiver signal P_r is calculated. The given loss can be translated to the channel transfer function $H(f)$, and after accounting for channel effects signal received $P_r(f)$ can be calculated using the equation:

$$P_r(f) = P_t(f)H(f). \tag{16}$$

Thus, received signal $x_r(t)$ can be calculated by accounting for the frequency selective channel response.

C. Receiver

At the receiver, to maximize the detection, we use two matched filters, one for the up-chirp and one for the down-chirp. The impulse response of an ideal matched filter is given by $h(t) = x_r(\tau - t)$, where $x_r(t)$ is the received signal at receiver. For the formulation of BER we also account for the noise added to the signal and this can be represented as $y(t) = x_r(t) + n(t)$, where $n_(t)$ is the additive white Gaussian noise. To perform the detection, the received signal is then multiplied with the corresponding up-chirp $s_1(t)$ and down-chirp $s_0(t)$ signal to produce detector outputs.

$$M_i = \sum_{t=0}^{T} y(t)s_i(t)dt, \quad i = 0, 1 \quad 0 \leq t \geq T \tag{17}$$

Comparing M_0 and M_1 we can identify the detected bit. If $M_0 > M_1$ detected bit is "0" and if $M_0 < M_1$ detected bit is "1". The cross-correlation coefficient ρ between up-chirp and down-chirp is defined as:

$$\rho = \frac{1}{\sqrt{E_b}} \sum_{t=0}^{T} s_0(t)s_1(t)dt, \tag{18}$$

where E_b is the energy per bit. For a standard chirp signal probability of error can be analytically expressed as [101], [103],

$$P_e = \frac{1}{2} erf\left(\frac{E_b}{2N_0}(1-\rho)\right), \tag{19}$$

where N_0 is noise power spectral density. The relation between signal to noise ratio (SNR), E_b and N_0 is given by:

$$SNR = \frac{R_b}{B}\frac{E_b}{N_0}, \tag{20}$$

where R_b is the bit rate, B is bandwidth, E_b is the energy per bit and N_0 is power spectral density of noise.

IX. Numerical Analysis

A. Antenna Chirp Excitation

The chirp signal, generated as per (7), is presented in Fig. 13. The generated signal spans from 180 THz to 250 THz over a sweep time of 2.5 ns. The power is equally distributed across the entire sweep frequency.

B. Imprinted Chirp Waveform

The generated chirp signal is then transmitted through the antenna. To account for the effect of the antenna response on the transmitted chirp, we calculated the transfer function of the antenna and calculated the power of the transmitted signal using (10). The transmitted signal power is plotted in Fig. 14. It can be observed that for binding and non-binding cases, the majority of the power of the transmitted signal is centered around the antenna resonant frequency.

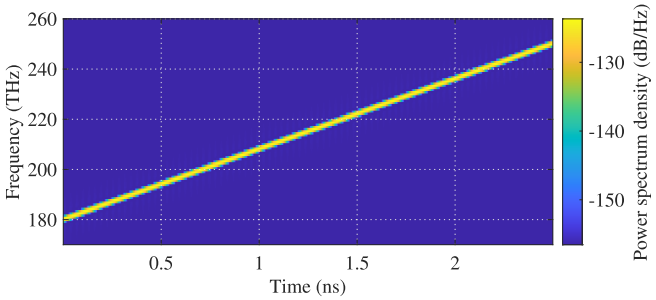

Fig. 13. Power spectrum of linear chirp signal used for antenna excitation.

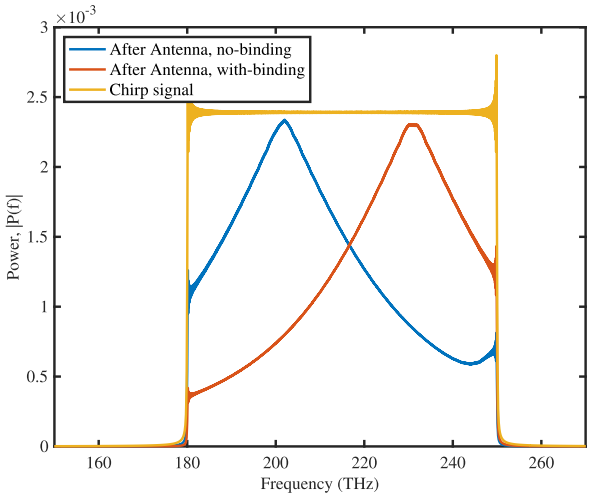

Fig. 14. Chirp signal power vs the response of antenna affecting the transmitted signal.

C. Chirp Sensing Detection

To successfully perform detection from the received signal, we compute the power and plot the power spectrum of the received signal. As shown in Fig. 15a for no biomarker binding case and Fig. 15b for biomarker binding case, the sensing features of binding vs. non-binding can be easily distinguished with a peak power cut-off of -127dB. The frequency shift from 200THz to 230THz demonstrates the use of an antenna with a chirp waveform for successful detection.

D. Joint Communication and Sensing

For joint sensing and communication analysis, the up-chip transmitted signal is modeled as bit 1 and down-chirp as bit 0. Using this symbol scheme, the data packet is encoded and transmitted. For illustration purposes, as an example, a reference transmitted packet "01001110" with binding is shown in Fig 16b. It can be observed that most of the power of the packet is transmitted in the antenna binding frequency band (f_1). These results for binding detection while up-chirp and down-chirp signals are also clearly distinguishable for successful data packet detection. Similarly, in Fig. 16a, the packet shown is transmitted in the absence of the biomarker and, similarly, the data is easily comprehensible.

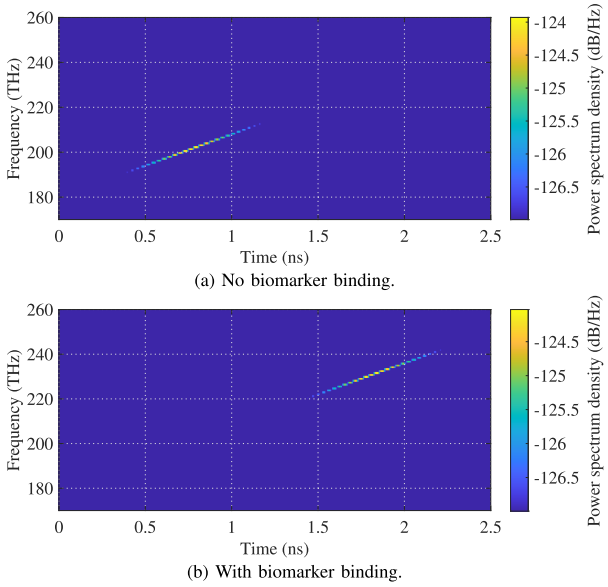

Fig. 15. Detection of antenna resonant frequency before and after binding based on the cutoff frequency and power spectrum.

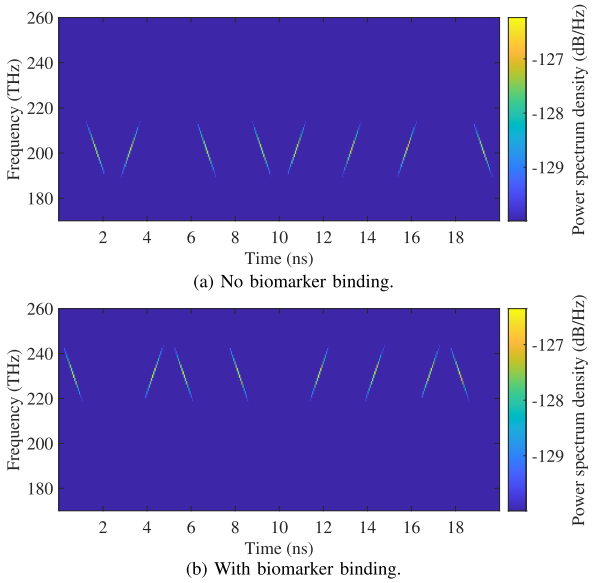

Fig. 16. Data packet (01001110) transmitted using chirp modulation scheme.

E. Performance Analysis at Edge

For the performance analysis of this proposed joint communication and sensing system, we performed the BER analysis simulation with 10,000 bits. We compared it with the analytical BER of a chirp-based communication system. Figure 17 shows the results of simulated analysis of antenna binding and non-binding cases from the sensor to wearable channel and benchmarks them with standard chirp performance for a given SNR. It can be observed that the performance is lower than standard chirp but still closely follows the analytical BER expression of chirp, demonstrating the ability of chirp waveform resilience for communications, even with the imprinted antenna binding features. Such loss of performance can be justified with the antenna's sensing response causing

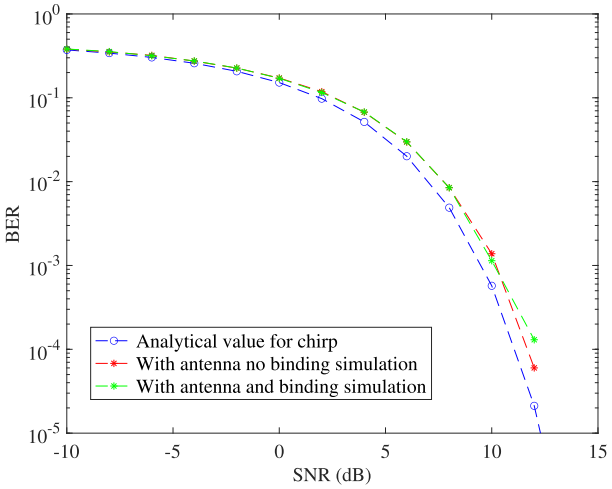

Fig. 17. BER analysis of the proposed joint communication and sensing waveform with human channel model.

additional losses to the transmitted chirp signal, thus increasing the required SNR to achieve the same BER.

F. Spectrum/Bandwidth Optimization

In the proposed scheme, there is a trade-off between the efficiency in which the spectral resources are utilized and the complexity of the solution to be implemented by a nanomachine. To tackle this trade-off, different system variations can be made to optimize either the complexity of implementation on a nano-node or the bandwidth occupied by the operational system. Such possible cases for optimization are as follows:

- **Case 1: Nanomachine complexity minimization.** In its current form, the presented scheme is aimed at reducing the nanomachine complexity while utilizing the entire bandwidth for chirp-based communication. This allows a wideband receiver with an up-chirp and down-chirp detector to perform signal detection and communication.
- **Case 2: Spectral efficiency maximization.** Given the performance of the antenna as a sensor discussed in Sec. IV, the frequencies of interest are f_0 (no binding) and f_1 (biomarker binding). To maximize the spectral efficiency, the nanomachine could transmit a narrow band signal first at f_0 and then at f_1, as part of a an initial Request-to-Send (RTS) in the context of a medium access control protocol for nanonetworks. These two signals could be compared by the receiver and followed by a clear to send (CTS) packet selecting the resonant band of the antenna. Therefore, if $P_{f_0} > P_{f_1}$, the next packet is sent at f_0. Thus, only the resonant antenna band is utilized for transmission to maximize spectral efficiency. The trade-off for such a scheme is that it requires a 2-way handshake before every data transmission to ensure detection can be reliably made. Such 2-way communication and MAC layer processing will add additional complexity to nanonode architecture. Additionally, if the antenna performs detection between the data packet being sent, it will require initiating a new handshake and might result in the loss of the data packet.
- **Case 3: Balancing complexity and spectral efficiency.** To balance the two previous cases, a solution that can minimize both complexity and bandwidth of operation while resisting the frequency selective channel is needed. Such a unidirectional system can be designed by sending two simultaneous chirps at center frequencies f_0 and f_1, each with bandwidth $X < (f_1 - f_0)/2$, namely, one chirp centered at f_0 (from $f0 - X/2$ to $f0 + X/2$) for the non-binding state and one chirp centered at f_1 (from $f1 - X/2$ to $f2 + X/2$) for the binding state. Thus, for any given transmission simultaneous sensing and detection can be performed. The detection results from detector design in the Fig. 11 can be used to select the data detection chirp frequency for minimal addition to the complexity and ease of operation. The required bandwidth X should be calculated using a detailed analysis of factors such as the bio-functional layer used, measured effective shift in antenna resonance with binding, and frequency selective nature of the channel for the band of operation. Therefore, ensuring a balanced and optimized operation of the proposed nano-system.

X. Conclusion

In this paper, we have proposed and numerically modeled a nano-patch-antenna-based joint communication and sensing system that, through the Internet of Nano-Bio Things architecture, bridges nanoscale networks with cloud computing through the edge. We investigated the use of a nano patch antenna as a sensor by modeling the effects of changing patch thickness and conductivity of the top layer of the antenna on its resonant frequency. We demonstrated that this change of resonating frequency could be utilized for simultaneous sensing and communication by using broadband chirp signals and performing a thorough numerical analysis. We proposed the detection mechanism that can be used for sensing by nanomachines. We performed a comprehensive analysis and benchmarked the communication performance to a standard chirp signal. We established the feasibility of a nano-sensing and communication system that offers the ability to perform edge sensing and can reduce the need for high computational resources required by the conventional spectrometric sensors while maintaining a minimal footprint on a nanomachine node.

References

[1] A. Sangwan and J. M. Jornet, "Joint nanoscale communication and sensing enabled by plasmonic nano-antennas," in *Proc. 8th Annu. ACM Int. Conf. Nanosc. Comput. Commun.*, Sep. 2021, pp. 1–6.
[2] F. Vollmer and L. Yang, "Review label-free detection with high-Q microcavities: A review of biosensing mechanisms for integrated devices," *Nanophotonics*, vol. 1, nos. 3–4, pp. 267–291, Dec. 2012.
[3] A. Shafiee, E. Ghadiri, J. Kassis, N. P. Zarandi, and A. Atala, "Biosensing technologies for medical applications, manufacturing, and regenerative medicine," *Current Stem Cell Rep.*, vol. 4, no. 2, pp. 105–115, Jun. 2018.
[4] J. Xu, H. Miao, J. Wang, and G. Pan, "Molecularly imprinted synthetic antibodies: From chemical design to biomedical applications," *Small*, vol. 16, no. 27, Jul. 2020, Art. no. 1906644.
[5] J. R. Mejía-Salazar and O. N. Oliveira, Jr., "Plasmonic biosensing: Focus review," *Chem. Rev.*, vol. 118, no. 20, pp. 10617–10625, Oct. 2018.
[6] M. I. Stockman, "Nanoplasmonic sensing and detection," *Science*, vol. 348, no. 6232, pp. 287–288, Apr. 2015.

[7] X. Zeng et al., "Plasmonic interferometer array biochip as a new mobile medical device for cancer detection," *IEEE J. Sel. Topics Quantum Electron.*, vol. 25, no. 1, pp. 1–7, Jan./Feb. 2018.

[8] P. Miao et al., "Orbital angular momentum microlaser," *Science*, vol. 353, pp. 464–467, Jul. 2016.

[9] P. Laferriere et al., "Multiplexed single-photon source based on multiple quantum dots embedded within a single nanowire," *Nano Lett.*, vol. 20, no. 5, pp. 3688–3693, May 2020.

[10] L. Liu, J. Dong, D. Gao, A. Zheng, and X. Zhang, "On-chip passive three-port circuit of all-optical ordered-route transmission," *Sci. Rep.*, vol. 5, no. 1, pp. 1–9, May 2015.

[11] D. Teng, Y. Yang, J. Guo, W. Ma, Y. Tang, and K. Wang, "Efficient guiding mid-infrared waves with graphene-coated nanowire based plasmon waveguides," *Results Phys.*, vol. 17, Jun. 2020, Art. no. 103169.

[12] Q. Liu et al., "Plasmonic waveguide design for the enhanced forward stimulated Brillouin scattering in diamond," *Sci. Rep.*, vol. 8, no. 11, p. 88, Jan. 2018.

[13] Y. Fang and M. Sun, "Nanoplasmonic waveguides: Towards applications in integrated nanophotonic circuits," *Light, Sci. Appl.*, vol. 4, no. 6, p. e294, Jun. 2015.

[14] R. W. Purnamaningsih, N. R. Poespawati, and E. Dogheche, "Design of a four-branch optical power splitter based on gallium-nitride using rectangular waveguide coupling for telecommunication links," *J. Eng.*, vol. 2019, Jul. 2019, Art. no. e7285305.

[15] S. Idres and H. Hashemi, "Low-power SiN thermo-optic phase modulator operating in red visible wavelength range," in *Proc. Conf. Lasers Electro-Opt.*, May 2022, pp. 1–2.

[16] M. Luo et al., "Aunps assisted all-fiber compact phase modulator and its application in erbium-doped fiber laser," *Opt. Commun.*, vol. 497, Oct. 2021, Art. no. 127186.

[17] M. Nafari and J. M. Jornet, "Modeling and performance analysis of metallic plasmonic nano-antennas for wireless optical communication in nanonetworks," *IEEE Access*, vol. 5, pp. 6389–6398, 2017.

[18] G. S. Unal and M. I. Aksun, "Bridging the gap between RF and optical patch antenna analysis via the cavity model," *Sci. Rep.*, vol. 5, no. 1, pp. 1–8, Nov. 2015.

[19] L. Novotny and N. van Hulst, "Antennas for light," *Nature Photon.*, vol. 5, no. 2, pp. 83–90, Feb. 2011.

[20] P. Bharadwaj, B. Deutsch, and L. Novotny, "Optical antennas," *Adv. Opt. Photon.*, vol. 1, no. 3, p. 438, Nov. 2009.

[21] H. Ren, X. Fang, J. Jang, J. Bürger, J. Rho, and S. A. Maier, "Complex-amplitude metasurface-based orbital angular momentum holography in momentum space," *Nature Nanotechnol.*, vol. 15, no. 11, pp. 948–955, Nov. 2020.

[22] M. Kadic, G. W. Milton, M. van Hecke, and M. Wegener, "3D metamaterials," *Nature Rev. Phys.*, vol. 1, no. 3, pp. 198–210, Mar. 2019.

[23] T. Ali, A. W. M. Saadh, R. C. Biradar, J. Anguera, and A. Andújar, "A miniaturized metamaterial slot antenna for wireless applications," *AEU, Int. J. Electron. Commun.*, vol. 82, pp. 368–382, Dec. 2017.

[24] I. F. Akyildiz, J. M. Jornet, and M. Pierobon, "Nanonetworks: A new frontier in communications," *Commun. ACM*, vol. 54, no. 11, pp. 84–89, Nov. 2011.

[25] W. K. Chen et al., "Design of galvanic coupling intra-body communication transceiver using direct sequence spread spectrum technology," *IEEE Access*, vol. 8, pp. 84123–84133, 2020.

[26] M. Li et al., "Comparable investigation of characteristics for implant intra-body communication based on galvanic and capacitive coupling," *IEEE Trans. Biomed. Circuits Syst.*, vol. 13, no. 6, pp. 1747–1758, Dec. 2019.

[27] F. V. Pop et al., "Novel pMUT-based acoustic duplexer for underwater and intrabody communication," in *Proc. IEEE Int. Ultrason. Symp. (IUS)*, Oct. 2018, pp. 1–4.

[28] L. Galluccio, A. Lombardo, S. Palazzo, and M. Reno, "Guiding ultrasonic waves across blood vessels to support intra-body networking," in *Proc. 5th ACM Int. Conf. Nanosc. Comput. Commun. (NANOCOM)*. New York, NY, USA: Association for Computing Machinery, Sep. 2018, pp. 1–6, doi: 10.1145/3233188.3233207.

[29] S. Basu, D. Mitra, B. Mandal, and R. Augustine, "Antenna based RF techniques for intrabody communication," in *IEEE MTT-S Int. Microw. Symp. Dig.*, Dec. 2020, pp. 1–4.

[30] H. Elayan, R. M. Shubair, J. M. Jornet, and P. Johari, "Terahertz channel model and link budget analysis for intrabody nanoscale communication," *IEEE Trans. Nanobiosci.*, vol. 16, no. 6, pp. 491–503, Sep. 2017.

[31] A. Sangwan and J. M. Jornet, "Beamforming optical antenna arrays for nano-bio sensing and actuation applications," *Nano Commun. Netw.*, vol. 29, Sep. 2021, Art. no. 100363.

[32] A. Sangwan, H. Pandey, P. Johari, and J. M. Jornet, "Increasing the communication distance between nano-biosensing implants and wearable devices," in *Proc. IEEE 19th Int. Workshop Signal Process. Adv. Wireless Commun. (SPAWC)*, Jun. 2018, pp. 1–5.

[33] B. Atakan, O. B. Akan, and S. Balasubramaniam, "Body area nanonetworks with molecular communications in nanomedicine," *IEEE Commun. Mag.*, vol. 50, no. 1, pp. 28–34, Jan. 2012.

[34] I. F. Akyildiz, F. Fekri, R. Sivakumar, C. R. Forest, and B. K. Hammer, "Monaco: Fundamentals of molecular nano-communication networks," *IEEE Wireless Commun.*, vol. 19, no. 5, pp. 12–18, Oct. 2012.

[35] I. F. Akyildiz, M. Pierobon, S. Balasubramaniam, and Y. Koucheryavy, "The internet of bio-nano things," *IEEE Commun. Mag.*, vol. 53, no. 3, pp. 32–40, Mar. 2015.

[36] T. Lister, P. A. Wright, and P. H. Chappell, "Optical properties of human skin," *J. Biomed. Opt.*, vol. 17, no. 9, Sep. 2012, Art. no. 090901.

[37] A. N. Bashkatov, E. A. Genina, and V. V. Tuchin, "Optical properties of skin, subcutaneous, and muscle tissues: A review," *J. Innov. Opt. Health Sci.*, vol. 4, no. 1, pp. 9–38, Jan. 2011.

[38] N. Bosschaart, G. J. Edelman, M. C. Aalders, T. G. van Leeuwen, and D. J. Faber, "A literature review and novel theoretical approach on the optical properties of whole blood," *Lasers Med. Sci.*, vol. 29, no. 2, pp. 453–479, Mar. 2014.

[39] S. Alaluf, D. Atkins, K. Barrett, M. Blount, N. Carter, and A. Heath, "Ethnic variation in melanin content and composition in photoexposed and photoprotected human skin," *PIGMENT CELL Res.*, vol. 15, no. 2, pp. 112–118, Apr. 2002.

[40] J. Riesz, "The spectroscopic properties of melanin," Ph.D. thesis, Univ. Queensland, 2007. [Online]. Available: https://www.semanticscholar.org/paper/The-spectroscopic-properties-of-melanin-Riesz/2e54aa265deabc58ae4bd26231c22356c6387681#citing-papers and https://api.semanticscholar.org/CorpusID:93075737

[41] P. Meredith, B. J. Powell, J. Riesz, S. P. Nighswander-Rempel, M. R. Pederson, and E. G. Moore, "Towards structure–property–function relationships for eumelanin," *Soft Matter*, vol. 2, no. 1, pp. 37–44, 2006.

[42] I. Pirovano et al., "Effect of adipose tissue thickness and tissue optical properties on the differential pathlength factor estimation for NIRS studies on human skeletal muscle," *Biomed. Opt. Exp.*, vol. 12, no. 1, pp. 571–587, Jan. 2021.

[43] E. Lazareva and V. Tuchin, "Blood refractive index modelling in the visible and near infrared spectral regions," *J. Biomed. Photon. Eng.*, vol. 4, no. 1, Mar. 2018, Art. no. 010503.

[44] H. Li, L. Lin, and S. Xie, "Refractive index of human whole blood with different types in the visible and near-infrared ranges," *Proc. SPIE*, vol. 3914, pp. 517–521, Jun. 2000. [Online]. Available: https://www.spiedigitallibrary.org/conference-proceedings-of-spie/3914/0000/Refractive-index-of-human-whole-blood-with-different-types-in/10.1117/12.388073.full

[45] P. Johari and J. M. Jornet, "Nanoscale optical wireless channel model for intra-body communications: Geometrical, time, and frequency domain analyses," *IEEE Trans. Commun.*, vol. 66, no. 4, pp. 1579–1593, Apr. 2018.

[46] J. Beuthan, O. Minet, J. Helfmann, M. Herrig, and G. Müller, "The spatial variation of the refractive index in biological cells," *Phys. Med. Biol.*, vol. 41, no. 3, pp. 369–382, Mar. 1996.

[47] A. M. Shrivastav, U. Cvelbar, and I. Abdulhalim, "A comprehensive review on plasmonic-based biosensors used in viral diagnostics," *Commun. Biol.*, vol. 4, no. 1, pp. 1–12, Jan. 2021.

[48] J. N. Anker, W. P. Hall, O. Lyandres, N. C. Shah, J. Zhao, and R. P. Van Duyne, "Biosensing with plasmonic nanosensors," in *Nanoscience and Technology*. London, U.K.: Macmillan, Aug. 2009, pp. 308–319.

[49] D. Rodrigo et al., "Mid-infrared plasmonic biosensing with graphene," *Science*, vol. 349, no. 6244, pp. 165–168, 2015. [Online]. Available: http://www.science.org/doi/10.1126/science.aab2051

[50] A. V. Kabashin et al., "Plasmonic nanorod metamaterials for biosensing," *Nature Mater.*, vol. 8, no. 11, pp. 867–871, Nov. 2009.

[51] C. F. Bohren, "How can a particle absorb more than the light incident on it?" *Amer. J. Phys.*, vol. 51, no. 4, pp. 323–327, Apr. 1983.

[52] A. B. Taylor and P. Zijlstra, "Single-molecule plasmon sensing: Current status and future prospects," *ACS Sensors*, vol. 2, no. 8, pp. 1103–1122, Aug. 2017.

[53] M. Moskovits, "Surface-enhanced spectroscopy," *Rev. Mod. Phys.*, vol. 57, no. 3, pp. 783–826, Jul. 1985.

[54] A. Kinkhabwala, Z. Yu, S. Fan, Y. Avlasevich, K. Müllen, and W. E. Moerner, "Large single-molecule fluorescence enhancements produced by a bowtie nanoantenna," *Nature Photon.*, vol. 3, no. 11, pp. 654–657, Nov. 2009.

[55] S. Fayyaz, M. Tabatabaei, R. Hou, and F. Lagugné-Labarthet, "Surface-enhanced fluorescence: Mapping individual hot spots in silica-protected 2D gold nanotriangle arrays," *J. Phys. Chem. C*, vol. 116, no. 21, pp. 11665–11670, May 2012.

[56] J. Jatschka, A. Dathe, A. Csáki, W. Fritzsche, and O. Stranik, "Propagating and localized surface plasmon resonance sensing—A critical comparison based on measurements and theory," *Sens. Bio-Sens. Res.*, vol. 7, pp. 62–70, Mar. 2016.

[57] Y. Huang, M.-K. Nguyen, A. K. Natarajan, V. H. Nguyen, and A. Kuzyk, "A DNA origami-based chiral plasmonic sensing device," *ACS Appl. Mater. Interfaces*, vol. 10, no. 51, pp. 44221–44225, Dec. 2018.

[58] V. Bochenkov and T. Shabatina, "Chiral plasmonic biosensors," *Biosensors*, vol. 8, no. 4, p. 120, Dec. 2018.

[59] W. A. Paiva-Marques, F. R. Gómez, O. N. Oliveira, and J. R. Mejía-Salazar, "Chiral plasmonics and their potential for point-of-care biosensing applications," *Sensors*, vol. 20, no. 3, p. 944, Jan. 2020.

[60] M. Dass, F. N. Gür, K. Kołątaj, M. J. Urban, and T. Liedl, "DNA origami-enabled plasmonic sensing," *J. Phys. Chem. C*, vol. 125, no. 11, pp. 5969–5981, Mar. 2021.

[61] E. S. Pfaffenbach, W. O. F. Carvalho, O. N. Oliveira, and J. R. Mejía-Salazar, "Design of nanoarchitectures for magnetoplasmonic biosensing with near-zero-transmittance conditions," *ACS Appl. Mater. Interfaces*, vol. 13, no. 50, pp. 60672–60677, Dec. 2021.

[62] V. T. Tran, J. Kim, L. T. Tufa, S. Oh, J. Kwon, and J. Lee, "Magnetoplasmonic nanomaterials for biosensing/imaging and *in vitro/in vivo* biousability," *Anal. Chem.*, vol. 90, no. 1, pp. 225–239, Jan. 2018.

[63] D. Regatos, B. Sepúlveda, D. Fariña, L. G. Carrascosa, and L. M. Lechuga, "Suitable combination of noble/ferromagnetic metal multilayers for enhanced magneto-plasmonic biosensing," *Opt. Exp.*, vol. 19, no. 9, pp. 8336–8346, Apr. 2011.

[64] N. P. Mauranyapin, L. S. Madsen, M. A. Taylor, M. Waleed, and W. P. Bowen, "Evanescent single-molecule biosensing with quantum-limited precision," *Nature Photon.*, vol. 11, no. 8, pp. 477–481, Aug. 2017.

[65] C. Lee, F. Dieleman, J. Lee, C. Rockstuhl, S. A. Maier, and M. Tame, "Quantum plasmonic sensing: Beyond the shot-noise and diffraction limit," *ACS Photon.*, vol. 3, no. 6, pp. 992–999, Jun. 2016.

[66] T.-T. Tran and A. Mulchandani, "Carbon nanotubes and graphene nano field-effect transistor-based biosensors," *Trends Anal. Chem.*, vol. 79, pp. 222–232, May 2016.

[67] H. Shi et al., "A symmetrical optical waveguide based surface plasmon resonance biosensing system," *Sens. Actuators B, Chem.*, vol. 185, pp. 91–96, Aug. 2013.

[68] M. Kaisti, "Detection principles of biological and chemical FET sensors," *Biosensors Bioelectron.*, vol. 98, pp. 437–448, Dec. 2017.

[69] M. S. Cheng and C.-S. Toh, "Novel biosensing methodologies for ultrasensitive detection of viruses," *Analyst*, vol. 138, no. 21, pp. 6219–6229, Sep. 2013.

[70] M. H. Pournaghi-Azar, F. Ahour, and M. S. Hejazi, "Direct detection and discrimination of double-stranded oligonucleotide corresponding to hepatitis C virus genotype 3a using an electrochemical DNA biosensor based on peptide nucleic acid and double-stranded DNA hybridization," *Anal. Bioanal. Chem.*, vol. 397, no. 8, pp. 3581–3587, Aug. 2010.

[71] M. S. Hejazi, M. H. Pournaghi-Azar, and F. Ahour, "Electrochemical detection of short sequences of hepatitis C 3a virus using a peptide nucleic acid-assembled gold electrode," *Anal. Biochem.*, vol. 399, no. 1, pp. 118–124, Apr. 2010.

[72] L. D. Tran, D. T. Nguyen, B. H. Nguyen, Q. P. Do, and H. Le Nguyen, "Development of interdigitated arrays coated with functional polyaniline/MWCNT for electrochemical biodetection: Application for human papilloma virus," *Talanta*, vol. 85, no. 3, pp. 1560–1565, Sep. 2011.

[73] X. Liu, Z. Cheng, H. Fan, S. Ai, and R. Han, "Electrochemical detection of avian influenza virus H5N1 gene sequence using a DNA aptamer immobilized onto a hybrid nanomaterial-modified electrode," *Electrochim. Acta*, vol. 56, no. 18, pp. 6266–6270, Jul. 2011.

[74] J. Kirsch, C. Siltanen, Q. Zhou, A. Revzin, and A. Simonian, "Biosensor technology: Recent advances in threat agent detection and medicine," *Chem. Soc. Rev.*, vol. 42, no. 22, pp. 8733–8768, 2013.

[75] Z. Altintas et al., "Detection of waterborne viruses using high affinity molecularly imprinted polymers," *Anal. Chem.*, vol. 87, no. 13, pp. 6801–6807, Jul. 2015.

[76] B. D. Gupta, A. M. Shrivastav, and S. P. Usha, "Surface plasmon resonance-based fiber optic sensors utilizing molecular imprinting," *Sensors*, vol. 16, no. 9, p. 1381, Sep. 2016.

[77] R. Yatabe, T. Onodera, and K. Toko, "Fabrication of surface plasmon resonance sensor surface with control of the non-specific adsorption and affinity for the detection of 2,4,6-trinitrotoluene using an antifouling copolymer," *Frontiers Bioeng. Biotechnol.*, vol. 2, p. 10, Apr. 2014.

[78] I. Buzzacchera et al., "Polymer brush-functionalized chitosan hydrogels as antifouling implant coatings," *Biomacromolecules*, vol. 18, no. 6, pp. 1983–1992, 2017.

[79] T. Yang et al., "Surface plasmon cavities on optical fiber end-facets for biomolecule and ultrasound detection," *Opt. Laser Technol.*, vol. 101, pp. 468–478, May 2018.

[80] C. W. Rossler, E. Ertin, and R. L. Moses, "A software defined radar system for joint communication and sensing," in *Proc. IEEE RadarCon (RADAR)*, May 2011, pp. 1050–1055.

[81] J. A. Zhang, A. Cantoni, X. Huang, Y. J. Guo, and R. W. Heath, Jr., "Framework for an innovative perceptive mobile network using joint communication and sensing," in *Proc. IEEE 85th Veh. Technol. Conf. (VTC Spring)*, Jun. 2017, pp. 1–5.

[82] M. Alloulah and H. Huang, "Future millimeter-wave indoor systems: A blueprint for joint communication and sensing," *Computer*, vol. 52, no. 7, pp. 16–24, Jul. 2019.

[83] C. B. Barneto, S. D. Liyanaarachchi, T. Riihonen, L. Anttila, and M. Valkama, "Multibeam design for joint communication and sensing in 5G new radio networks," in *Proc. IEEE Int. Conf. Commun. (ICC)*, Jun. 2020, pp. 1–6.

[84] Z. Ni, J. A. Zhang, X. Huang, K. Yang, and F. Gao, "Parameter estimation and signal optimization for joint communication and radar sensing," in *Proc. IEEE Int. Conf. Commun. Workshops (ICC Workshops)*, Jun. 2020, pp. 1–6.

[85] S. Buzzi, C. D'Andrea, and M. Lops, "Using massive MIMO arrays for joint communication and sensing," in *Proc. 53rd Asilomar Conf. Signals, Syst., Comput.*, Nov. 2019, pp. 5–9.

[86] E. F. Williams et al., "Distributed sensing of microseisms and teleseisms with submarine dark fibers," *Nature Commun.*, vol. 10, no. 1, p. 5778, Dec. 2019.

[87] N. J. Lindsey et al., "Fiber-optic network observations of earthquake wavefields," *Geophys. Res. Lett.*, vol. 44, no. 23, pp. 11792–11799, 2017.

[88] G. Marra et al., "Ultrastable laser interferometry for earthquake detection with terrestrial and submarine cables," *Science*, vol. 361, no. 6401, pp. 486–490, 2018. [Online]. Available: https://www-science-org.ezproxy.neu.edu/doi/full/10.1126/science.aat4458

[89] H. Sakamoto, Y. Minpou, T. Sawai, Y. Enami, and S.-I. Suye, "A novel optical biosensing system using Mach–Zehnder-type optical waveguide for influenza virus detection," *Appl. Biochem. Biotechnol.*, vol. 178, no. 4, pp. 687–694, Feb. 2016.

[90] M. A. Brusatori and P. R. Van Tassel, "Biosensing under an applied voltage using optical waveguide lightmode spectroscopy," *Biosensors Bioelectron.*, vol. 18, no. 10, pp. 1269–1277, Sep. 2003.

[91] S. W. Kwon et al., "The fabrication of polymer-based evanescent optical waveguide for biosensing," *Appl. Surf. Sci.*, vol. 255, no. 10, pp. 5466–5470, Mar. 2009.

[92] G. I. Stegeman, J. J. Burke, and D. G. Hall, "Nonlinear optics of long range surface plasmons," *Appl. Phys. Lett.*, vol. 41, no. 10, pp. 906–908, Nov. 1982.

[93] A. B. Constantine et al., "Antenna theory: Analysis and design," in *Microstrip Antennas*, 3rd ed. Hoboken, NJ, USA: Wiley, 2005.

[94] M. Min, R. Land, T. Paavle, T. Parve, P. Annus, and D. Trebbels, "Broadband spectroscopy of dynamic impedances with short chirp pulses," *Physiol. Meas.*, vol. 32, no. 7, p. 945, 2011.

[95] E. Gerecht, K. O. Douglass, and D. F. Plusquellic, "Chirped-pulse terahertz spectroscopy for broadband trace gas sensing," *Opt. Exp.*, vol. 19, no. 9, pp. 8973–8984, 2011.

[96] G. B. Park and R. W. Field, "Perspective: The first ten years of broadband chirped pulse Fourier transform microwave spectroscopy," *J. Chem. Phys.*, vol. 144, no. 20, May 2016, Art. no. 200901.

[97] L. Vangelista, "Frequency shift chirp modulation: The LoRa modulation," *IEEE Signal Process. Lett.*, vol. 24, no. 12, pp. 1818–1821, Dec. 2017.

[98] G. J. Tearney, M. E. Brezinski, B. E. Bouma, M. R. Hee, J. F. Southern, and J. G. Fujimoto, "Determination of the refractive index of highly scattering human tissue by optical coherence tomography," *Opt. Lett.*, vol. 20, no. 21, p. 2258, Nov. 1995.

[99] A. Roggan, K. Dörschel, O. Minet, D. Wolff, and G. Müller, "The optical properties of biological tissue in the near infrared wavelength range: Review and measurements," in *Laser-Induced Interstitial Thermotherapy*. Berlin, Germany, Jun. 1995, pp. 10–44.

[100] A. N. Bashkatov, E. A. Genina, V. I. Kochubey, and V. V. Tuchin, "Optical properties of human skin, subcutaneous and mucous tissues in the wavelength range from 400 to 2000 nm," *J. Phys. D, Appl. Phys.*, vol. 38, pp. 2543–2555, Aug. 2005.

[101] P. Sen, H. Pandey, and J. M. Jornet, "Ultra-broadband chirp spread spectrum communication in the terahertz band," *Proc. SPIE*, vol. 11390, May 2020, Art. no. 113900G.

[102] H. Guo, J. M. Jornet, Q. Gan, and Z. Sun, "Cooperative Raman spectroscopy for real-time *in vivo* nano-biosensing," *IEEE Trans. Nanobiosci.*, vol. 16, no. 7, pp. 571–584, Oct. 2017.

[103] X. Wang, M. Fei, and X. Li, "Performance of chirp spread spectrum in wireless communication systems," in *Proc. 11th IEEE Singap. Int. Conf. Commun. Syst.*, Nov. 2008, pp. 466–469.

Amit Sangwan (Member, IEEE) received the Bachelor of Technology degree in electronics and communication engineering from the Guru Jambheshwar University of Science and Technology, India, in 2013, and the Master of Science degree in electrical engineering from the University at Buffalo, The State University of New York, Buffalo, NY, USA, in 2017. He is currently pursuing the Ph.D. degree with the Department of Electrical and Computer Engineering, Northeastern University, Boston, MA, USA, under the guidance of Dr. Josep Miquel Jornet. He worked as a Research and Development Engineer at an innovative start-up company in India from August 2013 to June 2015. He was a Visiting Researcher at Mitsubishi Electric Research Labs (MERL), Boston, in 2018. His research interests include the Internet of Things (IoT), nano-sensor networks, nano-optical antennas, beamforming arrays, ultra-broadband communications, nanophotonic systems, wireless optical communications, and bio-nano implant communications.

Josep Miquel Jornet (Senior Member, IEEE) received the B.S. degree in telecommunication engineering and the M.Sc. degree in information and communication technologies from the Universitat Politecnica de Catalunya, Barcelona, Spain, in 2008, and the Ph.D. degree in electrical and computer engineering from the Georgia Institute of Technology (Georgia Tech), Atlanta, GA, USA, in 2013. From August 2013 to August 2019, he was a Faculty Member with the Department of Electrical Engineering, University at Buffalo, The State University of New York. He is currently an Associate Professor with the Department of Electrical and Computer Engineering, the Director of the Ultrabroadband Nanonetworking Laboratory, and a member of the Institute for the Wireless Internet of Things as well as the SMART Center at Northeastern University, Boston, MA, USA, since 2019. His research interests include terahertz communication networks, wireless nano-bio-communication networks, and the Internet of Nano-Things. In these areas, he has coauthored more than 160 peer-reviewed scientific publications, one book, and has also been granted four U.S. patents. He was a recipient of the National Science Foundation CAREER Award and several other awards from IEEE, ACM, UB, and Northeastern University. Since July 2016, he has been the Editor-in-Chief of the *Nano Communication Networks* (Elsevier) journal. He is serving as the lead PI for multiple grants from U.S. federal agencies, including the National Science Foundation, the Air Force Office of Scientific Research, and the Air Force Research Laboratory.